EUROPEAN ORGANIZATION FOR NUCLEAR RESEARCH

CERN-EP/81-01
14 January 1981

DIFFRACTION DISSOCIATION IN PROTON-PROTON COLLISIONS AT ISR ENERGIES

J.C.M.Armitage, P.Benz*), G.J.Bobbink, F.C.Erne, P.Kooijman**)
P.K.Loebinger, A.A.Macbeth, H.E.Montgomery, P.G.Murphy,
A.Rudge, J.C.Sens, D.Stork+), J.Timmer.

CERN-Geneva, Switzerland
Daresbury Laboratory, U.K.
Foundation for Fundamental Research of Matter (FOM)
The Netherlands
University of Manchester, U.K.
University of Utrecht, The Netherlands.

ABSTRACT

Data are presented on the reaction $pp \to pX$ in the range of four-momentum transfer squared $0.04 < -t < 0.80$ GeV^2 and of centre of mass (CM) energy squared $550 < s < 3880$ GeV^2. Invariant cross sections are given as a function of M^2/s, where M is the mass of the missing system X, and of t. The cross sections are shown to scale in the variable M^2/s, for $M^2/s > 0.01$. The total diffractive cross section integrated over t and M^2/s up to $M^2/s = 0.05$ rises by approximately 15% from $\sigma_{dif} = 6.5 \pm 0.2$ mb at 550 GeV^2 to $\sigma_{dif} = 7.5 \pm 0.3$ mb at 3880 GeV^2.

Submitted to Nuclear Physics B

---

*) Deceased

+) Now at UKAEA, Culham Laboratory, U.K.

**) Now at ANL, Argonne Ill 60439, U.S.A.

The experiment presented in this paper is an extension of previous work on inclusive diffraction dissociation at the CERN ISR by the CERN-Holland-Lancaster-Manchester collaboration [1]. The present experiment extends the range in t down to $t=-0.04$ GeV^2 for $s<1480$ GeV^2 and provides data in the range $0.15<-t<0.8$ GeV^2 for CM energies of 2000, 2880 and 3880 GeV^2 .It therefore allows for the first time a reliable determination of the integrated single diffractive cross section over the same range of energies, over which the total cross section for pp scattering has been shown to be rising with energy [6].

The experimental setup has been described previously in detail [2] and consisted of a magnetic spectrometer with momentum resolution $\sigma(p)/p$ as given in table I, and a set of scintillation counter hodoscopes covering 97% of the full solid angle. One of the hodoscopes, consisting of 12 small overlapping counters, was placed directly opposite the spectrometer in the CM, and was used for identification of elastically scattered protons. The spectrometer was mobile in the vertical plane and could thus provide a continuous scan in production angle, Θ , down to 10 mrad.

Data were taken at eight values of s, corresponding to the five standard ISR momenta (11.8,15.4,22.5,26.8,31.6 GeV) colliding with an 11.8 GeV beam travelling towards the spectrometer and three combinations of equal ISR momenta in both beams (22.5/22.5,26.8/26.8,31.6/31.6 GeV). At all energies a scan was made with $10<\Theta<35$ mrad. The values of s

and the ranges in θ and t are summarized in Table I. Because of requirements of other ISR users the data at the three highest energies were taken with the Terwilliger beam adjustment scheme applied. In this scheme the primary beams are narrowed down horizontally from 5 to 1 cm width, thereby reducing the interaction volume to a few cm .

In the reaction

$$p_1 + p_2 \rightarrow p_3 + X$$

the square of the momentum transfer t and the mass squared of the system X, M^2, are given by

$$t=(p_3-p_2)^2$$

and $$M^2=(p_1+p_2-p_3)^2$$

where p is the four-momentum of particle i and 2 is the initial proton travelling towards the spectrometer and 3 is the detected particle. For each event the values of t and M^2 were determined using the measured three-momentum of the detected particle and assuming the mass to be that of the proton. (Previous measurements show the contamination from particles other than the proton to be smaller than 0.1% [4]) In non-Terwilliger conditions the momenta of the initial protons were deduced by extrapolating the measured track back to the horizontal planes of the ISR beams and using the known horizontal position dependence of the momenta inside the ISR beams. For Terwilliger conditions this information was lost and the initial momenta were taken to be the weighted mean of the beam momenta before the Terwilliger scheme was applied.

At each value of M^2 and t the number of events due to elastic scattering was deduced from the topology of the charged particles which accompanied the spectrometer particle. Elastic events were identified by the criterion that one and only one charged particle was detected in addition to the spectrometer particle and that the two particles were collinear in the CM. Corrections were made for particles traversing two counters, interactions in the material of the vacuum chamber and random counts. The accuracy of the determination of the number of elastic events was of the order 1-2%. These elastic events were used to calibrate the momentum scale and measure the resolution $\sigma(p)$ (see Table I).

The data were normalized by comparing the number of measured elastic events to previously published differential elastic cross sections. Where no data on elastic scattering were available (at s=1050, 1260 and 1480 GeV^2) the elastic cross sections were obtained through interpolation by fitting the exponential slopes of the published differential cross sections at $-t<0.14$ GeV^2 and $-t>0.14$ GeV^2 as linear functions in lns and the intercept at $t=0.0$ GeV^2 as a quadratic function in lns. A fuller description of the normalisation procedure is given in Ref.5.

Fig. 1 shows the invariant cross section versus M^2/s for several values of t, for the five lowest s values. The resolution of the spectrometer is equal at all these s

values and so allows a direct comparison of the data. Fig. 1 shows that the data scale in the variable M^2/s for values of $M^2/s>0.01$. To investigate whether scaling holds at higher energies all data were convoluted with gaussian resolution functions to simulate the resolution of the spectrometer at the highest s value. Fig. 2 shows the data thus treated for s=550,2000 and 2880 GeV^2 together with the data at s=3880 GeV^2 for several values of t. It is again seen that the data scale for $M^2/s>0.01$ Fig. 3a and b show the data integrated in t and M^2/s. For Fig. 3a the integration limits in M^2/s are $-\infty<M^2/s<0.01$ and for Fig. 3b the limits are $0.01<M^2/s<0.05$. (The data in these figures have been corrected for the varying resolution of the spectrometer). For $M^2/s>0.01$ the data show no s dependance (scaling) whereas for $M^2/s<0.01$ there is a clear increase of the cross section with increasing s. This apparent non scaling for $M^2/s<0.01$ is kinematic in origin and due to the fact that the minimum mass, M_{min}, that can be produced is $M_{min}=m_p+m_\pi$, independent of s. This is borne out in Fig. 3c, which shows that the position of the peak in the M^2/s scale varies linearly with 1/s.

The t-dependence of the data, when integrated from the lower limit in M^2 up to $M^2/s=0.05$ is shown in Fig.4 for all values of s along with data from our previous experiment [1]. It can be parameterised as

$$d\sigma/dt=A\ \exp(bt+ct^2)$$

Integration with a procedure described in ref.1, and

multiplication by a factor 2 because of the symmetric case, pp->Xp, then gives the total diffractive cross section. The integration limit $M^2/s=0.05$ is chosen to balance the small contribution expected from higher M^2/s values against a contamination from non-diffractive processes at lower M^2/s values. For comparison with literature data the cross sections integrated up to $M^2/s=0.1$ were also computed. Fig. 5a and b show the total cross section as a function of s for both limits of integration and Table II gives the numerical values. Fig.5b also shows the diffractive cross sections as obtained by several FNAL experiments [7-9]. There is good agreement where the data overlap.

In the figure are also shown several hypotheses for the energy dependence of the diffractive cross section. The dashed line shows the total inelastic cross section with a constant subtracted so as to make it equal to the measured diffractive cross section at $s=1050$ GeV^2. It is clear that for neither integration limit the rise in the diffractive cross section can fully explain the rise in the total inelastic cross section. The solid curves show the best fit to the data assuming the diffractive cross section is a fixed fraction of the total cross section. This hypothesis gives good agreement with the data with $\sigma_{dif}\ (M^2/s<0.05)=(0.17\pm0.01)\sigma_{tot}$ and $\sigma_{dif}\ (M^2/s<0.1)=(0.19\pm0.02)\sigma_{tot}$. Finally the dot-dash line represents the prediction of the energy-dependence of diffractive scattering as derived from a parton model formulation by Miettinen and Pumplin [10].

In this model the elastic, diffractive and total cross sections are given as functions of two parameters. These parameters are fixed using the total and total elastic cross sections and the model then predicts the magnitude of the diffractive cross section. The agreement in absolute magnitude of the cross section is reasonably good, the prediction lying between the values for the two different integration limits. The prediction that the cross section rises by 0.8 mb from $s=550$ GeV^2 to $s=3880$ GeV^2 is in excellent agreement with the measured value of 1 mb.

In conclusion, we have presented data on inelastic diffractive scattering at the highest energies currently available and have shown that the data scale in M^2/s for $M^2/s>0.01$. The diffractive peak shifts toward lower values of M^2/s as s increases, consistent with the lower limit for diffraction being fixed in M.

The t-dependence shows no indication of a vanishing cross section at $t=0.0$ GeV^2.

The total diffractive cross section rises by ~15% in the energy range $550<s<3880$ GeV^2 consistent with the predictions of the parton model of Miettinen and Pumplin and also with the hypothesis that diffraction scattering is a fixed fraction of the total cross section. The data rule out the the possibility that the rise in the diffractive cross section accounts for the total rise of the inelastic cross section.

A fuller analysis of the data and tables of cross

sections are presented in Ref.5.

We are grateful to the ISR Experimental Support, Vacuum, Operations, Power and Survey groups for assistance. This experiment was supported by the Nederlandse Organisatie voor Zuiver Wetenschappelijk Onderzoek through F.O.M. and by the U.K. Science Research Council through Daresbury Laboratory.

TABLES:

I : Momentum resolution, momentum transfer and production angle ranges for the data of this experiment.

II : Total diffractive cross sections for integration limits $M^2/s<0.05$ and $M^2/s<0.1$.

FIGURE CAPTIONS:

1 : Invariant cross section versus M^2/s for several values of t and for $550<s<1480$ GeV^2.

2 : Invariant cross section versus M^2/s for several values of t and for s=550,2000,2880 and 3880 GeV^2. The data at the three lowest energies have been convoluted with gaussians to simulate the worse resolution of the spectrometer at s=3880 GeV^2.

3a: Invariant cross section integrated over t for $M^2/s<0.01$ versus 1/s.

3b: invariant cross section integrated over t for $0.01<M^2/s<0.05$ versus 1/s.

3c: Position of the maximum of the diffractive peak in M^2/s as a function of 1/s.

4 : The inelastic differential cross section versus t after integration in mass from threshold up to $M^2/s=0.05$.

5 : Integrated diffractive cross section for

(a) $M^2/s<0.05$

and (b) $M^2/s<0.10$.

(+) data from present experiment and ref 1.

(×) data from Ref.7, (◇) data from Ref.8 and (□) data from Ref.9. Dashed line σ_{inel}-const normalised to the measured cross section at s=1050 GeV^2.

Solid line $A\sigma_{tot}$, with A=0.17 (a) and A=0.19 (b).

Dot-dash line prediction of the parton model of Miettinen and Pumplin [10].

TABLE I

MOMENTA		s	$\sigma(p)/p$	θ-range	$\|t\|$-range
BEAM1 GeV	BEAM2 GeV	GeV^2	%	mrad	GeV^2
11.8	11.8	550	0.70	10-35	0.0275-0.270
15.4	11.8	750	0.70	10-35	0.0375-0.190
22.5	11.8	1050	0.70	10-40	0.0425-0.270
26.8	11.8	1260	0.70	15-35	0.1050-0.330
31.6	11.8	1480	0.70	13-35	0.0750-0.330
22.5	22.5	2000	0.94	10-45	0.0900-0.840
26.8	26.8	2880	1.05	10-40	0.1100-0.840
31.6	31.6	3880	1.45	10 35	0.1100-0.840

TABLE II

s GeV^2	$\sigma_{dif}(M^2/s<0.05)$ mb	$\sigma_{dif}(M^2/s<0.10)$ mb
550	6.5 ± 0.2	7.8 ± 0.4
750	6.3 ± 0.2	7.6 ± 0.4
1050	6.5 ± 0.2	7.8 ± 0.5
1260	7.5 ± 0.5	8.9 ± 0.6
1480	7.3 ± 0.4	8.8 ± 0.5
2000	7.3 ± 0.3	8.9 ± 0.4
2880	7.0 ± 0.3	8.6 ± 0.4
3880	7.5 ± 0.3	9.1 ± 0.4

REFERENCES:

[1] M.G.Albrow et al. Nucl.Phys. B108 (1976) 1

[2] J.C.Armitage et al. Nucl.Phys. B132 (1978) 365

[3] K.Terwilliger Proc. Int. Conf. on High Energy Accelerators. p.53. (CERN, 1959)

[4] J.Singh et al. Nucl.Phys. B140 (1978) 189

[5] P.Kooijman University of Utrecht, Ph.D.Thesis (1979)

[6] U.Amaldi et al. Phys.Lett. 66B (1977) 390 and references therein.

[7] J.Chapman et al. Phys Rev. Lett. 32 (1971) 257

[8] K.Dao et al. Phys. Lett. 45B (1973) 399

[9] J.Schamberger et al. Phys. Rev. D17 (1978) 1268, Phys.Rev.Lett. 34 (1975) 1121

[10] H.Miettinen and J.Pumplin Phys.Rev. D18 (1978) 1696

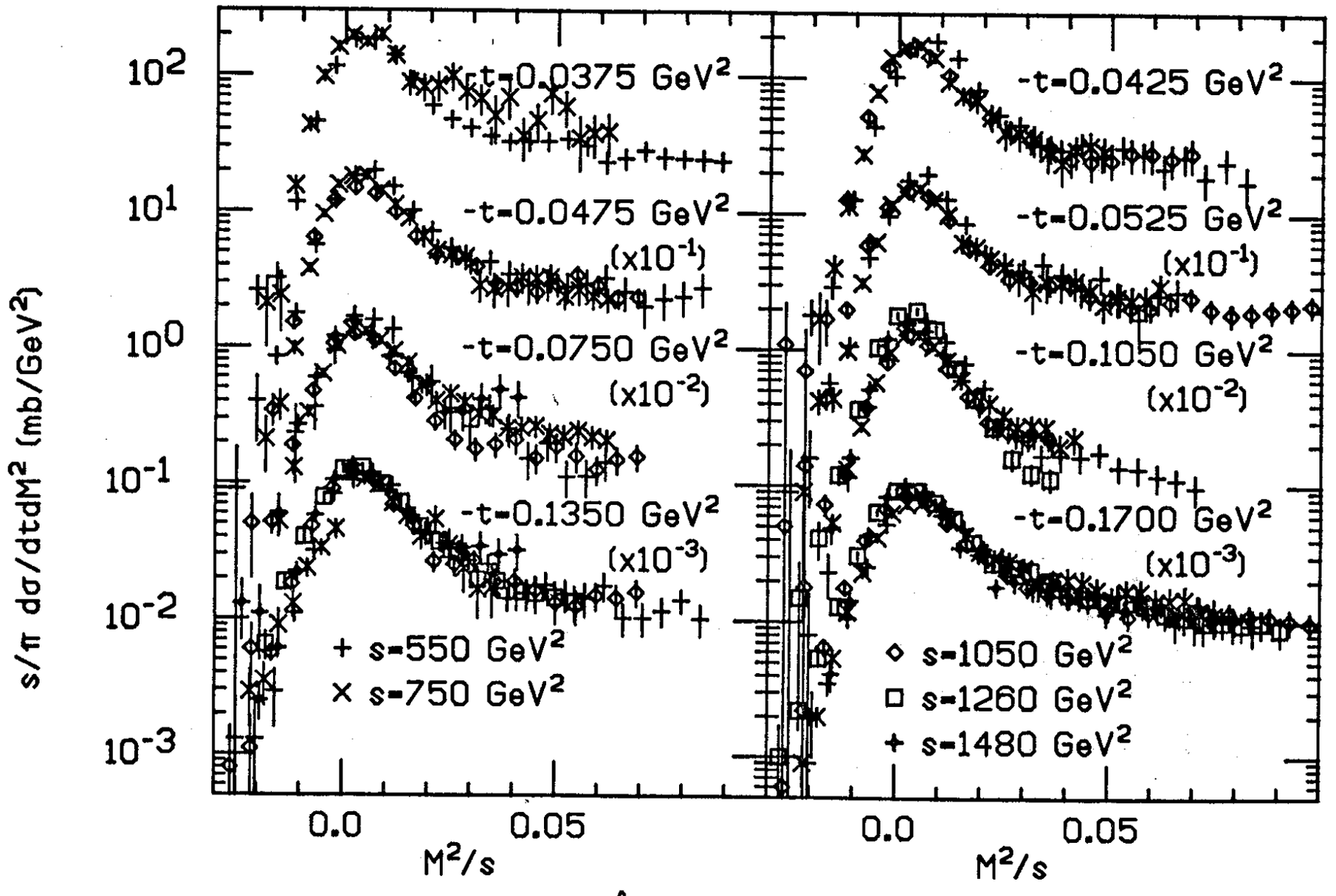
10^2
10^1
10^0
10^{-1}
10^{-2}
10^{-3}
$s/\pi\ d\sigma/dtdM^2$ (mb/GeV^2)
-t=0.0375 GeV^2
-t=0.0475 GeV^2
(x10^{-1})
-t=0.0750 GeV^2
(x10^{-2})
-t=0.1350 GeV^2
(x10^{-3})
+ s=550 GeV^2
× s=750 GeV^2
-t=0.0425 GeV^2
-t=0.0525 GeV^2
(x10^{-1})
-t=0.1050 GeV^2
(x10^{-2})
-t=0.1700 GeV^2
(x10^{-3})
◇ s=1050 GeV^2
□ s=1260 GeV^2
+ s=1480 GeV^2
0.0
0.05
M^2/s
0.0
0.05
M^2/s

fig. 1

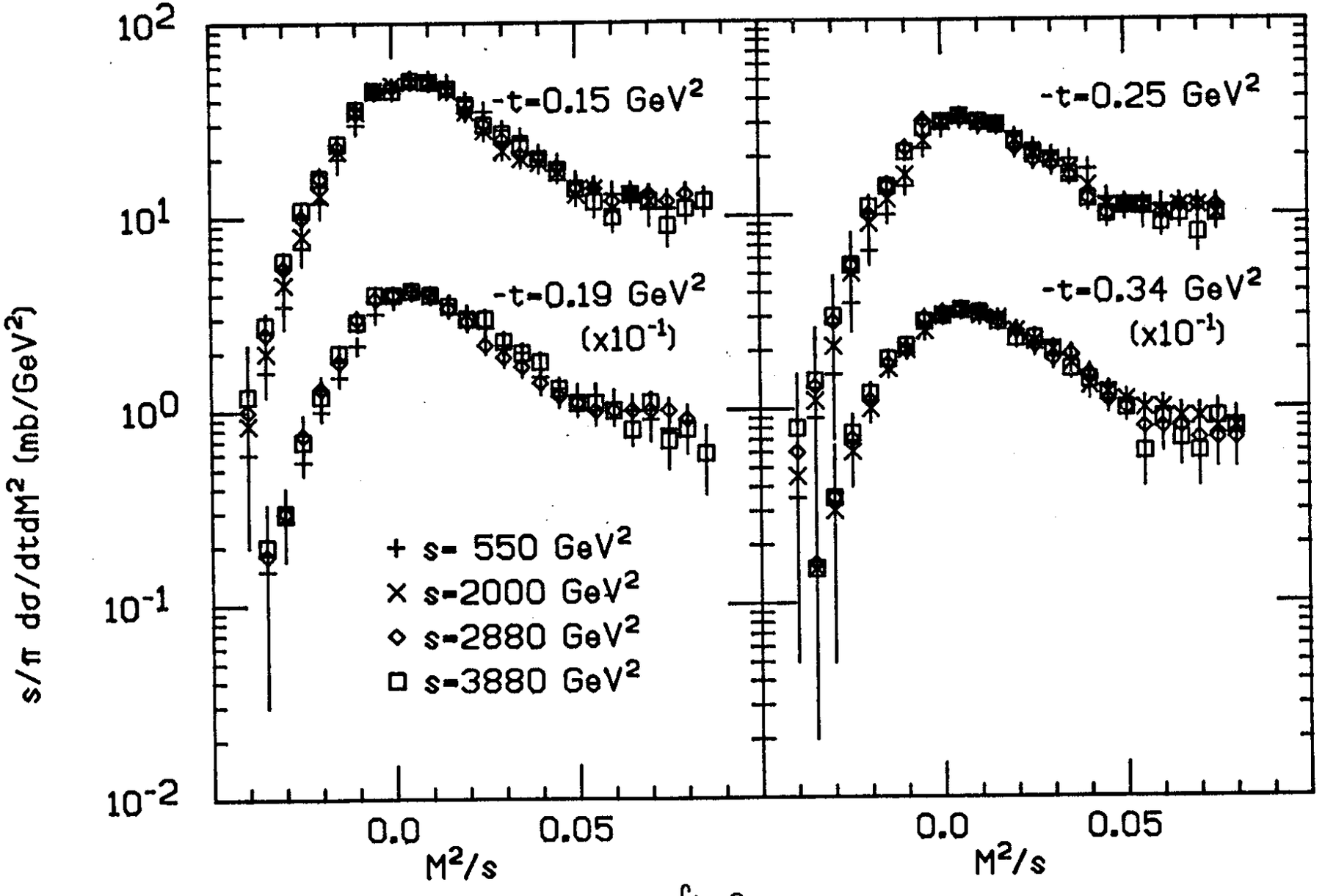
10^2
10^1
10^0
10^{-1}
10^{-2}
$s/\pi\ d\sigma/dtdM^2$ (mb/GeV^2)
-t=0.15 GeV^2
-t=0.19 GeV^2
(x10^{-1})
-t=0.25 GeV^2
-t=0.34 GeV^2
(x10^{-1})
+ s= 550 GeV^2
× s=2000 GeV^2
◇ s=2880 GeV^2
□ s=3880 GeV^2
0.0
0.05
M^2/s
0.0
0.05
M^2/s

fig.2

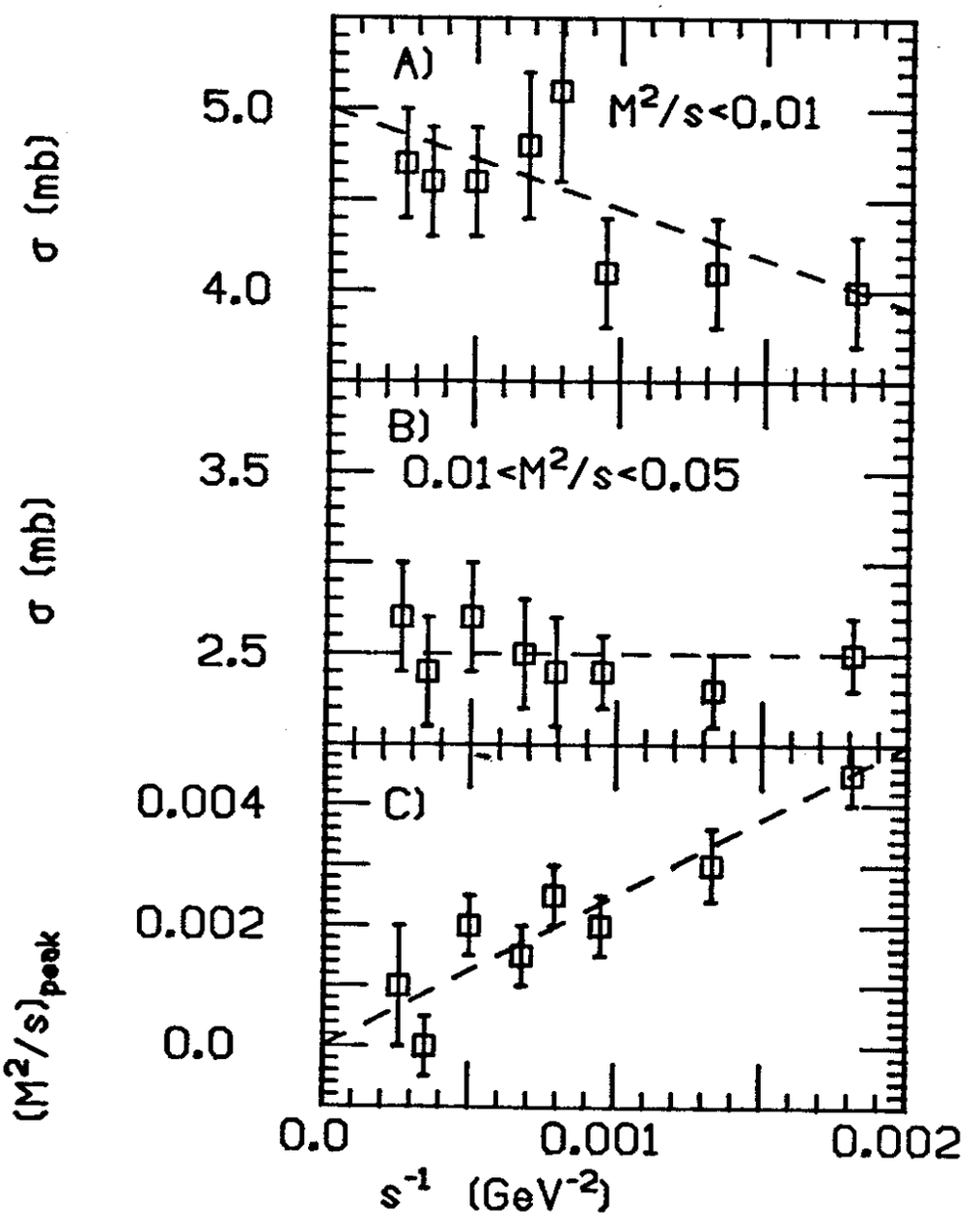
A)
$M^2/s<0.01$
5.0
4.0
σ (mb)
B)
$0.01<M^2/s<0.05$
3.5
2.5
σ (mb)
C)
0.004
0.002
0.0
$(M^2/s)_{peak}$
0.0
0.001
0.002
s^{-1} (GeV^{-2})

fig. 3

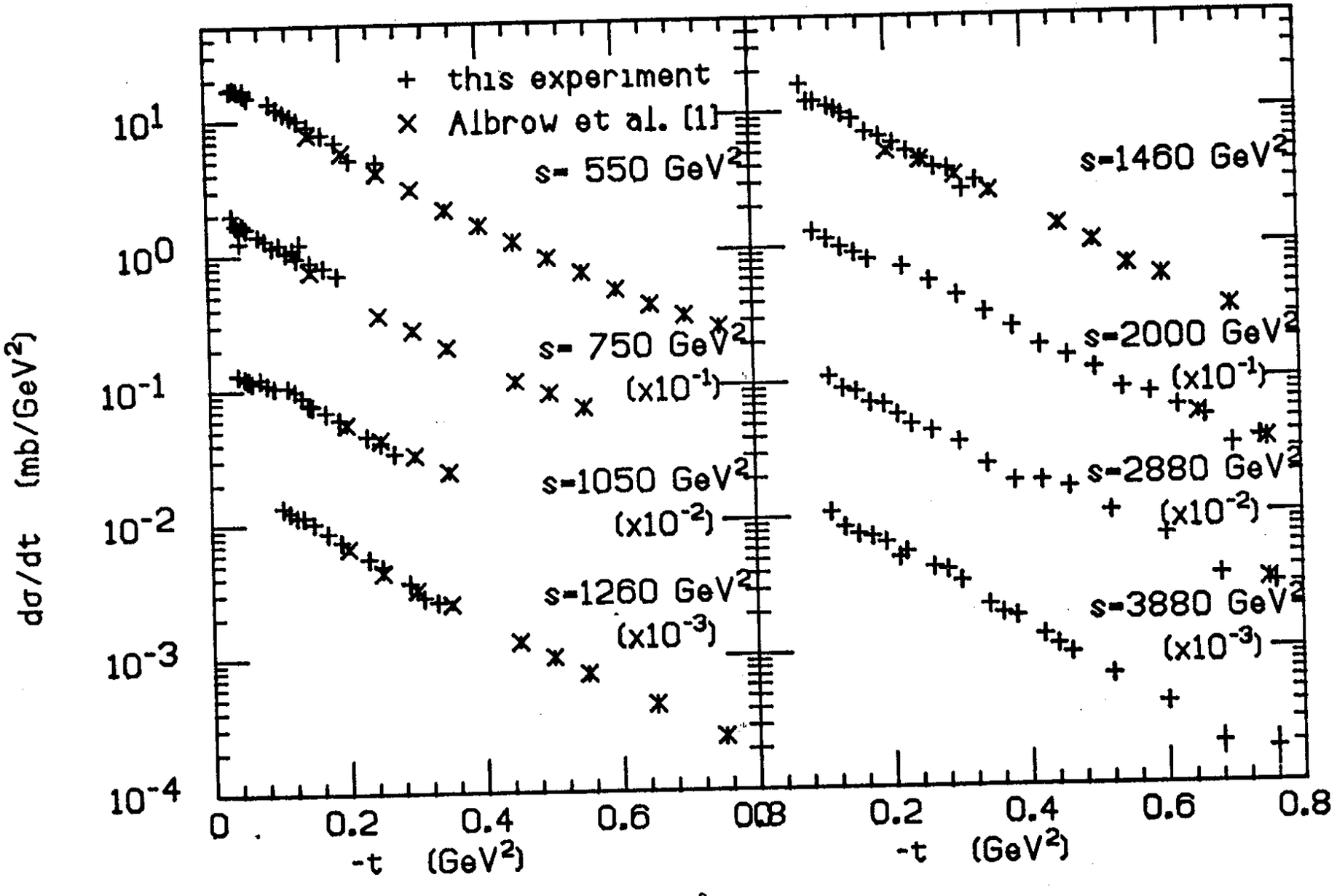
+ this experiment
× Albrow et al. [1]
s= 550 GeV²
s= 750 GeV²
(x10⁻¹)
s=1050 GeV²
(x10⁻²)
s=1260 GeV²
(x10⁻³)
s=1460 GeV²
s=2000 GeV²
(x10⁻¹)
s=2880 GeV²
(x10⁻²)
s=3880 GeV²
(x10⁻³)
dσ/dt (mb/GeV²)
-t (GeV²)
-t (GeV²)

fig. 4

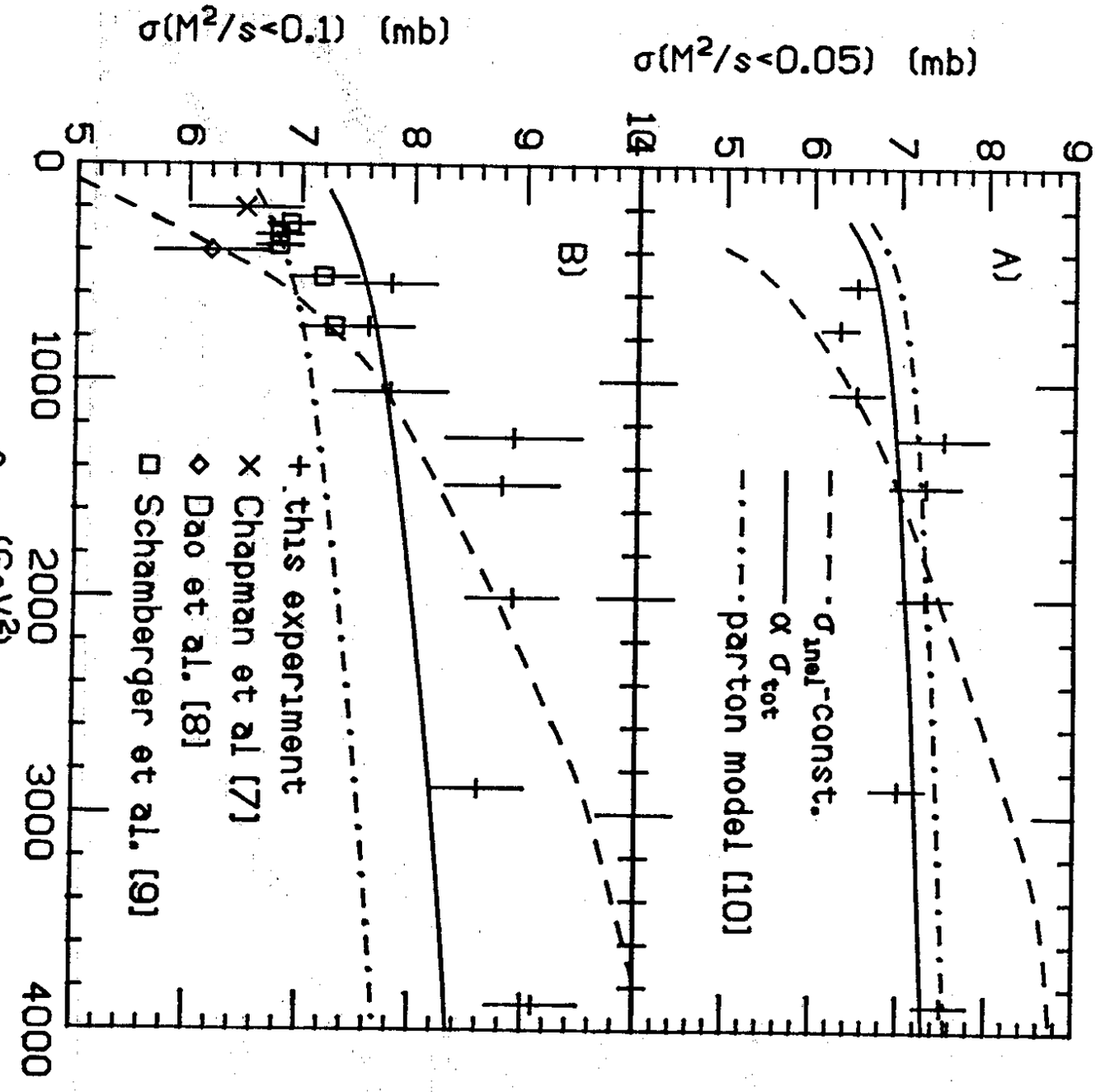
σ(M²/s<0.05) (mb)
σ(M²/s<0.1) (mb)
A)
B)
parton model [10]
σ_inel-const.
α σ_tot
this experiment
Chapman et al [7]
Dao et al. [8]
Schamberger et al. [9]
s (GeV²)

fig. 5.